OXFORD

Human Molecular Genetics, 2019, Vol. 28, No. 10 1738–1751

doi: 10.1093/hmg/ddz012
Advance Access Publication Date: 28 January 2019
General Article

GENERAL ARTICLE

Systemic investigation of bone and muscle abnormalities in dystrophin/utrophin double knockout mice during postnatal development and the mechanisms

Xueqin Gao[1,2,3], Ying Tang[2], Sarah Amra[1], Xuying Sun[1], Yan Cui[1], Haizi Cheng[1], Bing Wang[2] and Johnny Huard[1,2,3,*]

[1]Department of Orthopaedic Surgery, McGovern Medical School, University of Texas Health Science Center at Houston, Houston, TX, USA, [2]Department of Orthopaedic Surgery, University of Pittsburgh, Pittsburgh, USA and [3]Steadman Philippon Research Institute, Vail, CO, USA

*To whom correspondence should be addressed at: 1881 East Road, South Campus Research Building 3, Room 3SCR6.3618, Houston, TX 77054, USA. Tel: 713-486-5429; Fax: 713-796-9697; Email: Johnny.Huard@uth.tmc.edu

Abstract

The dystrophin$^{-/-}$utrophin$^{-/-}$ double knockout (dKO-Hom) mouse is a murine model of human Duchenne muscular dystrophy. This study investigated the bone and muscle abnormalities of dKO-Hom mouse and mechanisms. We collected bone and skeletal muscle samples from control mice and three muscular dystrophic mouse models at different ages and performed micro-computer tomography and histological analyses of both bone and skeletal muscle tissues. Serum receptor activator of nuclear factor kappa-B ligand (RANKL) and sclerostin (SOST) levels, osteoclastogenesis and serum proteomics were also analyzed. Our results indicated that dKO-Hom mice developed skeletal muscle histopathologies by 5 days of age, whereas bone abnormalities developed at 4 weeks of age. Furthermore, our results indicated that the numbers of osteoblasts and osteoclasts were decreased in the proximal tibia and spine trabecular bone of dKO-Hom mice compared to wild-type (WT) mice, which correlated with a significant reduction in serum RANKL levels. The number of tibia cortical osteocytes also decreased, whereas serum SOST levels increased significantly in dKO-Hom mice than WT mice. Osteoblastic number was significantly lower, but osteoclast number increased, in the spine L6 of dKO-Hom mice than WT mice at 6 weeks of age, resulting in a decrease in bone formation and an increase in bone resorption. Serum proteomics results revealed abnormal proteome profiles in dKO-Hom mice compared to control mice. In conclusion, our study elucidated the timing of development of bone and muscle abnormalities. The bone abnormalities in dKO-Hom mice are correlated with lower serum RANKL and higher SOST levels that resulted in dysregulation of osteogenesis and osteoclastogenesis and bone loss.

Introduction

Duchenne muscular dystrophy (DMD) is a severe muscle wasting disease caused by mutations in the dystrophin gene. Often, DMD patients become wheelchair-bound by 12 years of age due to skeletal muscle wasting (1–5). The *mdx* mouse, which is a murine model for human DMD, has a single base mutation in the dystrophin gene that results in the loss of dystrophin expression

Received: September 7, 2018. **Revised:** January 4, 2019. **Accepted:** January 8, 2019

in the sarcolemma of myofibers (6). It has been shown that *mdx* mice exhibit lower mineral bone density and biomechanical properties at 21 days of life, even when muscle damage is not apparent at this stage (7). It has also been demonstrated that *mdx* mouse femurs have lower strength, stiffness and energy absorption capacity (7). Anna Rufo *et al.* reported that, in 6-month-old *mdx* mice, the tibia trabecular bone volume/total volume ration (BV/TV) and trabecular number (Tb.N) was significantly lower, whereas trabecular separation (Tb.Sp) was significantly higher, compared to control mice. In addition, osteoclast numbers were significantly increased, and osteoblast numbers were significantly decreased, in tibial trabecular bone in *mdx* mice, compared to normal age-matched mice. Similarly, in the calvarial bone of *mdx* mice, the osteoclast surface/bone surface and osteoclast numbers were significantly increased, but osteoblast numbers did not change, relative to control mice. In addition, the levels of serum receptor activator of nuclear factor kappa-B ligand (RANKL) were lower, and those of interleukin 6 (IL-6) were higher, in *mdx* mice compared to normal mice. Similar bone abnormalities have been observed in DMD patients (8). It has also been shown that 3-month-old *mdx* mice subjected to non-stabilized fracture exhibited delayed tibial fracture healing due to chronic inflammation (9). Inhibition of inflammation could reverse these bone abnormalities in healing without affecting bone and cartilage (9).

However, another study has shown that young *mdx* mice exhibited spontaneous bone healing in a 2 mm calvarial bone defect model (10). Although *mdx* mice treated with prednisolone or restricted activity exhibited a ~7% decrease in bone strength, bone stiffness decrease was only observed in mice with restricted activity. The intrinsic properties of bone, including volumetric bone mineral density and modulus of elasticity, were not affected by either treatment (11).

Interestingly, *mdx* mice have a normal life span and do not exhibit severe muscle degeneration as seen in human patients, due to utrophin expression, which compensates for the lack of dystrophin. In 1997, Joshua R. Sanes' group reported on their development of the dystrophin/utrophin double knockout (dKO-Hom) mouse model (12), which more closely mimics the clinical manifestations seen in DMD patients. This model has also been shown to be more suitable for gene therapy testing for DMD (13).

dKO-Hom mice have been shown to exhibit severe muscle damage, including continuous degeneration/regeneration, inflammation and necrosis and ectopic calcification via stem cell depletion, activation of non-myogenic mesenchymal stem cells and different signaling pathways, such as Notch and RhoA (14–18). dKO-Hom mice also demonstrated a spectrum of severe bone abnormalities at 6 weeks of age (19). However, it is unknown how early the bone abnormalities developed, whether the severe bone abnormalities in this dKO-Hom mouse model happened before or after muscle damage, and what are the mechanisms that prompt the current study.

Results

The onset of skeletal muscle histopathologies occurred at 5 days after birth while no bone abnormalities was observed in the dKO-Hom mouse model

At 5 days of age, our results indicate minimal muscle fiber regeneration and focal inflammatory cell infiltration by hematoxylin and eosin (H&E) staining in the different muscle groups analyzed, including the skeletal muscles of skull (lower jaw muscle), spine, femur and tibia for *mdx*, dKO-Het and dKO-Hom mice, compared to wild-type (WT) mice (Fig. 1A). Although skeletal muscle histopathology was observed, we did not observe any heterotopic bone formation in *mdx*, dKO-Het or dKO-Hom mice in comparison to WT control mice (Supplementary Material, Fig. S1). We collected bone tissues from different locations and analyzed the bone microarchitecture. For the proximal tibia, the BV/TV, density, Tb.N and Tb.Sp were not significantly different between dKO-Hom mice and the other groups. The trabecular thickness (Tb.Th) was significantly higher in dKO-Hom mice compared to WT control mice (Fig. 1B, E–I). There were no significant differences found for spine trabecular parameters, such as BV/TV, density, Tb.N, Tb.Th and Tb.Sp between dKO-Hom mice, and WT, *mdx* and dKO-Het mice (Fig. 1C, J–N). For the femur midshaft cortical bone, we found that *mdx* and dKO-Het mice had significantly higher cortical thickness (Ct.Th) than WT mice. No significant difference was found between dKO-Hom mice and the other groups (Fig. 1D, O–P). H&E staining of bone tissues indicated no abnormalities in the general bone structure for dKO-Hom mice in comparison with WT, *mdx* and dKO-Het mice (Supplementary Material, Fig. S2). Herovici's staining showed no differences in bone matrix collagen type I in the skull parietal bone, spine L6, femur cortical or proximal tibia between dKO-Hom mice and WT, *mdx* and dKO-Het mice (Supplementary Material, Fig. S3).

Lack of bone abnormalities in 2-week-old dystrophic mice while muscle damage persists

Based on the results of H&E staining, we found that muscle pathology persisted in all skeletal muscle groups tested at 2 weeks of age (Supplementary Material, Fig. S4). Microcomputer tomography (MicroCT) analysis of the proximal tibia indicated that the bone density of trabecular bone was significantly decreased in dKO-Hom mice compared to WT mice, whereas no significant differences were observed for BV/TV, Tb.N, Tb.Th or Tb.Sp between dKO-Hom mice and WT, *mdx* and dKO-Het mice (Supplementary Material, Fig. S5A–F). For the spine L6, microCT 3D images showed no apparent differences between dKO-Hom mice and the other groups. Quantification indicated that the BV/TV, BV density, Tb.N, Tb.Th and Tb.Sp in dKO-Hom mice were not significantly different when compared to the other mouse groups (Supplementary Material, Fig. S5G–L). For femur cortical bone, we found no significant differences in Ct.Th between dKO-Hom mice and WT, *mdx* and dKO-Het mice and any other two groups (Supplementary Material,Fig. S5M–N). H&E staining showed no abnormalities in general structural morphology of skull parietal bone, spine L6, femur cortical bone and proximal tibia in the four groups of mice (Supplementary Material, Fig. S6). Herovici's staining showed no differences in collagen type 1 between dKO-Hom mice and WT, *mdx* and dKO-Het mice (Supplementary Material, Fig. S7). These results indicate that skeletal muscle pathology appeared earlier than bone abnormalities in the dKO-Hom mouse model.

Bone microarchitecture was significantly impaired in 4-week-old dKO-Hom mice

At 4 weeks of age, we found very severe pathological changes in all muscle groups (skull, spine, femur and tibia muscle groups) in *mdx*, dKO-Het and dKO-Hom mice, when compared to WT mice. These pathological changes included muscle fiber damage and regeneration (central nuclei, yellow arrows), inflammation (black arrows) and fibrosis and heterotopic bone formation

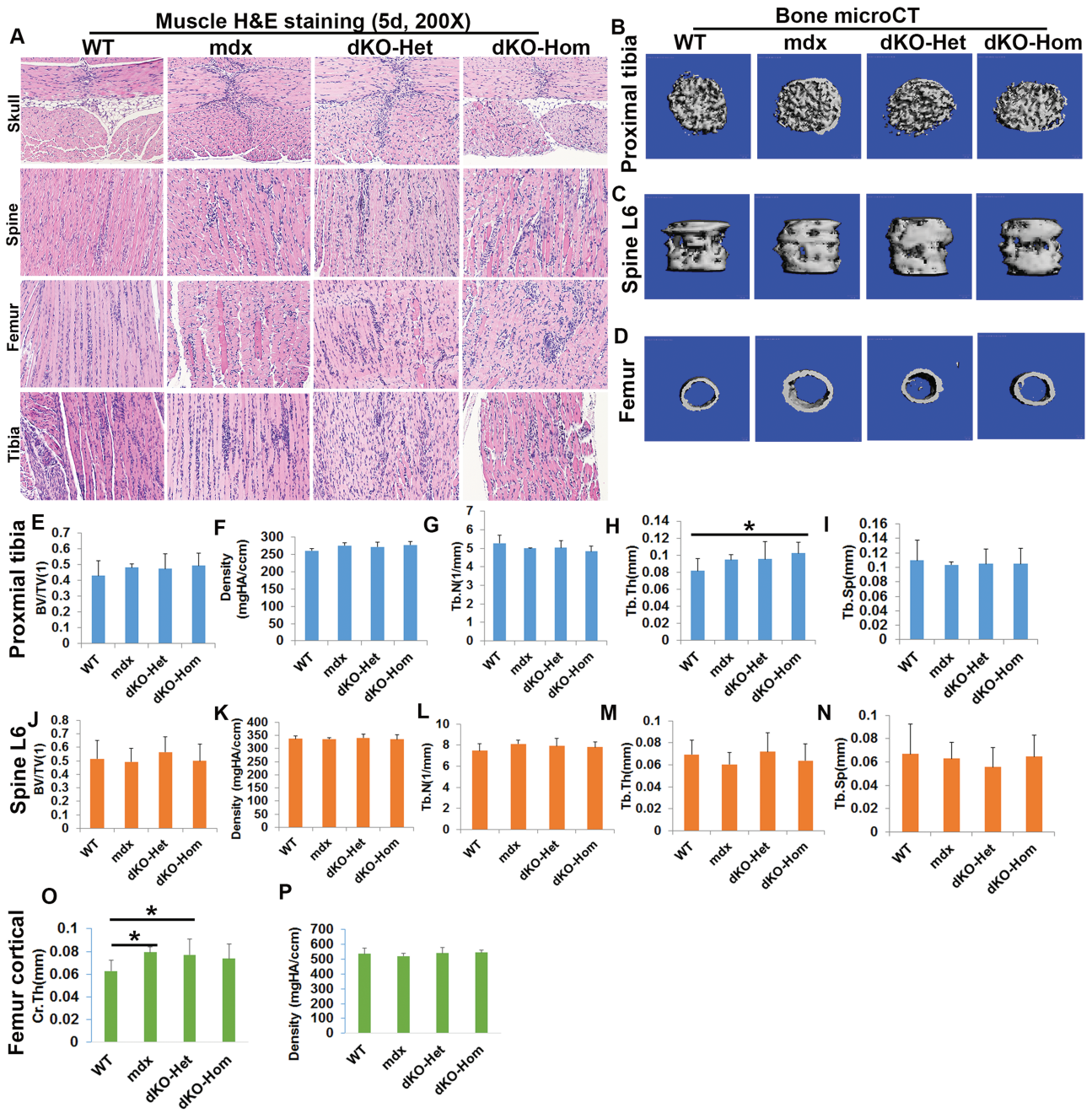

Figure 1. Characterization of skeletal muscle and bone of 5-day-old WT, mdx, dKO-Het and dKO-Hom mice. (**A**) H&E staining (200×) of different skeletal muscle tissue samples from each of the four groups of mice. Mild muscle necrosis and central nucleated muscle fibers are observed in the skull (lower jaw muscle), spine, femur and tibial skeletal muscle for *mdx*, dKO-Het and dKO-Hom mice. (**B–D**) MicroCT images of the proximal tibia (30 slices, top view), lumbar spine 6 (spine L6) and midshaft cortical bone of the femur from the four groups of mice. (**E–I**) MicroCT quantification of BV/TV, density, Tb.N, Tb.Th and Tb.Sp of the trabecular bone of the proximal tibia. No differences were found in BV/TV, BV density, Tb.N and Tb.SP between dKO-Hom, dKO-Het, *mdx* and WT mice. The Tb.Th of dKO-Hom mice was significantly higher than that of WT mice (*$P < 0.05$). (**J–N**) MicroCT quantification of BV/TV, density, Tb.N, Tb.Th and Tb.Sp of trabecular bone of spine L6 showed no difference between the dKO-Hom mice and other groups. (**O**). Femur Ct.Th was significantly higher in *mdx* and dKO-Het mice than in WT mice (*$P < 0.05$), whereas no significant differences were found between dKO-Hom mice and other groups. (**P**) dKO-Hom mice showed no differences in femur cortical bone density compared to WT, *mdx* and dKO-Het mice.

(green arrows) in *mdx*, dKO-Het and dKO-Hom mice compared to WT control mice (Fig. 2A). MicroCT analyses also showed heterotopic bone formation in the skeletal muscle of skull, spine, femur and tibia (Fig. 2B). MicroCT 3D images of the proximal tibia showed lower trabecular bone quality in the dKO-Hom mice (Fig. 3A). Quantification of bone microarchitecture of proximal tibia indicated that the dKO-Hom mice had significantly lower trabecular bone BV/TV, Tb.N and Tb.Th, and higher Tb.Sp than the other mouse groups (Fig. 3B, D–F). The BV density of dKO-Hom mice was significantly lower than *mdx*, dKO-Het mice and WT control mice (Fig. 3C). Similarly, microCT 3D images showed that the trabecular bone of spine L6 appeared less dense in dKO-Hom mice compared to WT, *mdx* and dKO-Het mice (Fig. 3G). After quantification, we found that spine L6 trabecular bone

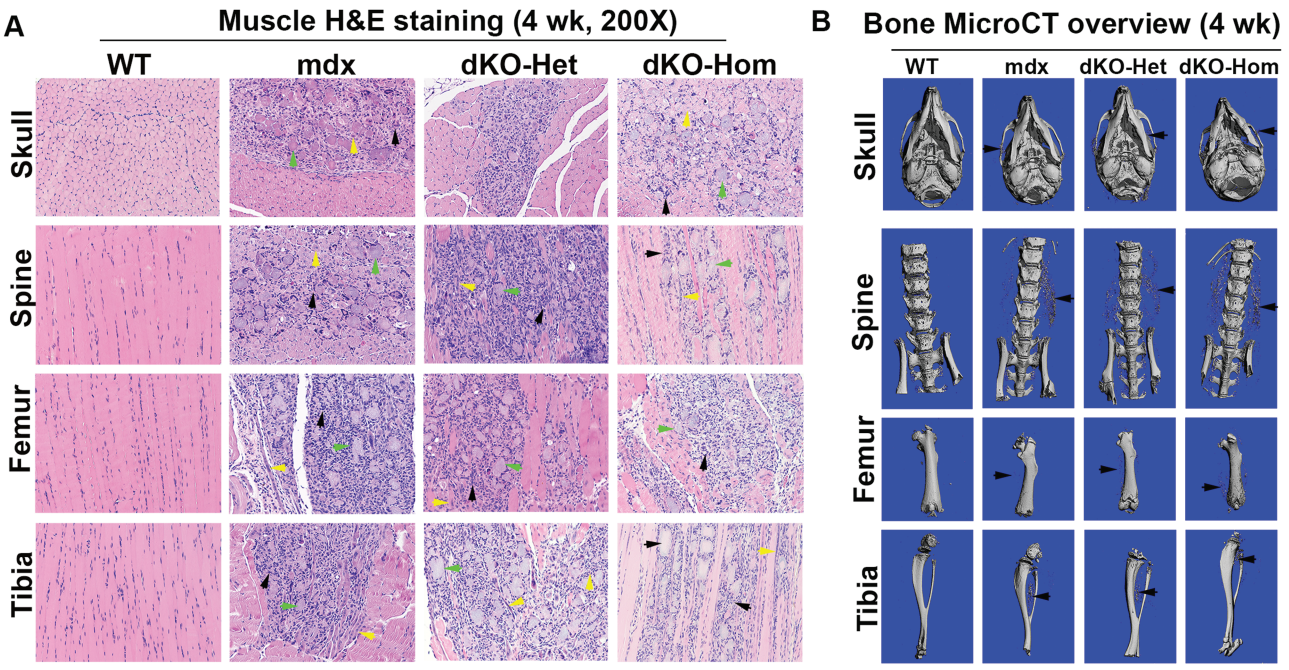

Figure 2. Characterization of skeletal muscle and bone of 4-week-old WT, *mdx*, dKO-Het and dKO-Hom mice. (**A**) H&E staining (200×) of different skeletal muscle tissue samples from each of the four groups of mice. Consistently, severe muscle damage, centrally nucleated myofibers (yellow arrows) and inflammation (green arrows) were found in the surrounding skeletal muscle of skull (lower jaw muscle), spine, femur and tibia in *mdx*, dKO-Het and dKO-Hom mice. Bony structures were identified in all muscle groups, with the exception of the WT control mice (black arrows). (**B**) MicroCT 3D overview of bone tissue at 4 weeks of age. Bone structures appeared normal in *mdx*, dKO-Het and dKO-Hom mice compared to WT control mice, with the exception that heterotopic bone formation was universally observed for *mdx*, dKO-Het and dKO-Hom mice in all bone surrounding muscle tissues imaged, as shown by black arrows in each representative image.

BV/TV, Tb.N and Tb.Th were significantly lower, and Tb.Sp was significantly higher, in dKO-Hom mice compared to the other mouse groups (Fig. 3H, J–L). The spine L6 trabecular bone density was significantly lower in dKO-Hom mice compared to *mdx*, dKO-Het mice and WT mice (Fig. 3I). Furthermore, the femur Ct.Th was smaller in dKO-Hom mice than in *mdx* and dKO-Het mice, and WT mice, as indicated by microCT 3D images and quantification (Fig. 3M–N). H&E staining showed no abnormalities in the bone structure of skull parietal bone, tibia, spine and femur; however, the trabecular bone of spine L6 and the proximal tibia was smaller in dKO-Hom mice than WT, mdx and dKO-Het mice (Supplementary Material, Fig. S8). Furthermore, Herovici's staining showed that bone matrix collagen type I was less dense in dKO-Hom mice compared to WT, *mdx* and dKO-Het mice. No differences were observed among the other groups of mice (Supplementary Material, Fig. S9).

Decreased in osteoblasts, osteoclasts and osteocytes number in dKO-Hom mice at 4 weeks old

To further investigate the mechanism(s) involved in lower bone microarchitecture in dKO-Hom mice, we studied the following three important bone cell types with respect to bone development and maintenance: osteoblasts, osteocytes and osteoclasts, via immunohistochemistry with osteocalcin, sclerostin (SOST) and tartrate-resistant acid phosphatase (TRAP) staining, respectively. We detected a significant reduction in the numbers of osteocalcin-positive osteoblasts in the trabecular bone of the proximal tibia in dKO-Hom mice when compared to WT mice (Fig. 4A–B). Moreover, we also found a reduction in the number of osteocalcin-positive osteoblasts in the trabecular bone of spine L6 of dKO-Hom mice compared to WT, *mdx* and dKO-Het mice (Fig. 4C–D). Furthermore, our results indicated that the number of TRAP-positive osteoclasts in the trabecular bone of the proximal tibia was significantly lower in dKO-Hom mice than in WT, *mdx* and dKO-Het mice. Additionally, the osteoclast number in the trabecular bone of the proximal tibia in dKO-Het mice was significantly lower than in WT mice (Fig. 4E–F). The osteoclast number in the trabecular bone of spine L6 was significantly lower in dKO-Hom mice than in WT, *mdx* and Het-mice (Fig. 4G–H). The $SOST^{+}$ osteocyte number was significantly lower in the tibial cortical bone of dKO-Hom mice compared to *mdx*, dKO-Het and WT mice (Fig. 4I–J).

Osteopenia in dKO-Hom mice at 4 weeks old is related to lower RANKL level and osteoclastogenesis

We performed *in vitro* osteoclastogenesis assays with bone marrow cells from the tibia and femur of 4-week-old mice. We found that the number of TRAP-positive multinuclear cells was lower among bone marrow cells from *mdx*, dKO-Het and dKO-Hom mice, after 7 days of culture in osteoclastogenesis differentiation media, compared to WT mice (Fig. 5A). We also found lower levels of Cathpsin K (CatK) and TRAP messenger ribonucleic acid (mRNA) in bone marrow cells from *mdx*, dKO-Het and dKO-Hom mice, relative to WT control mice, after 5 days of culture; however, the difference was not statistically significant (Fig. 5B). The results of enzyme-linked immunosorbent assay (ELISA) showed that serum RANKL levels were significantly lower in *mdx*, dKO-Het and dKO-Hom mice relative to WT mice (Fig. 5C). Furthermore, serum SOST levels were significantly higher in dKO-Hom mice than in WT mice (Fig. 5D).

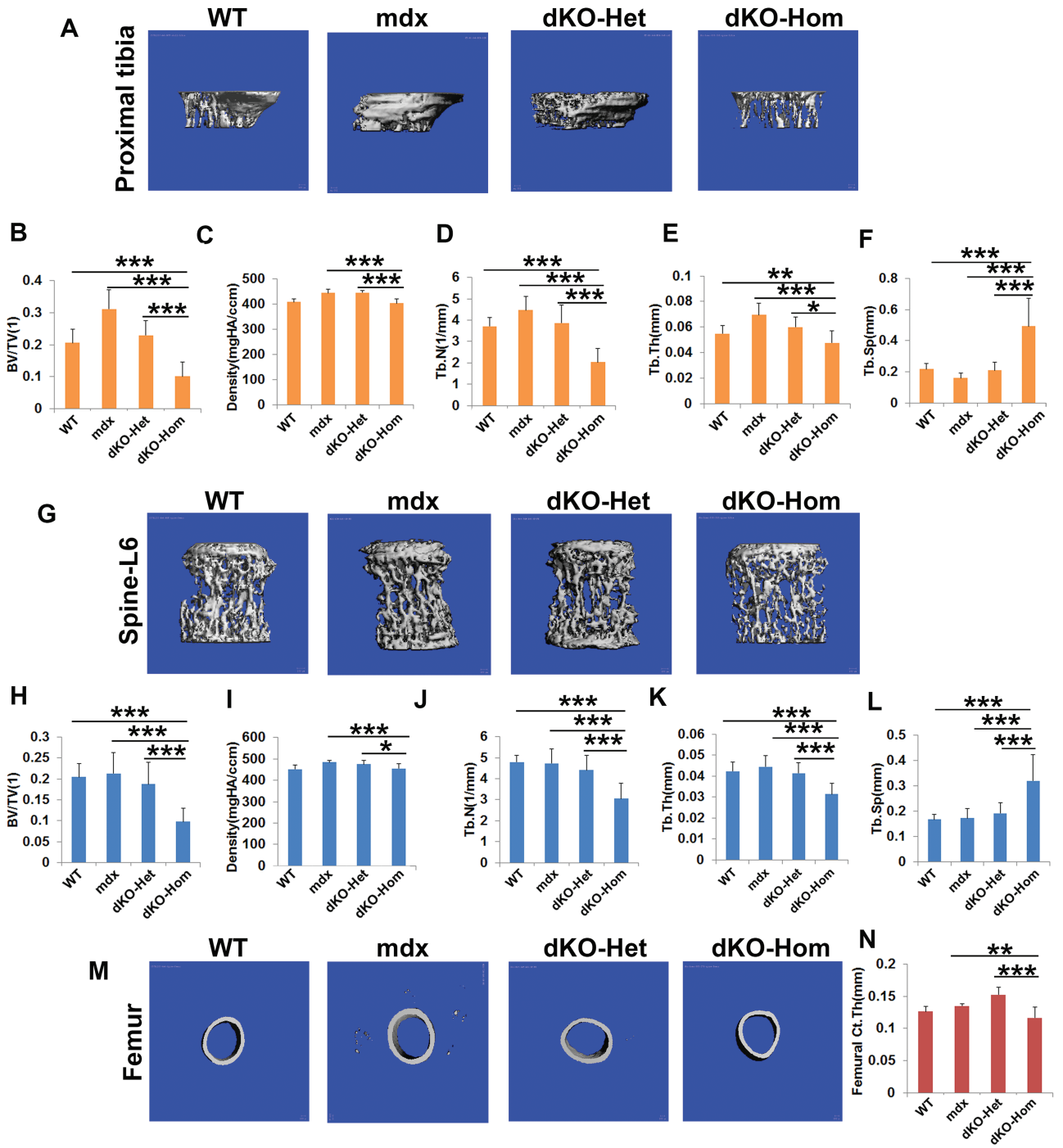

Figure 3. MicroCT analysis of bone microarchitecture in 4-week-old WT, *mdx*, dKO-Het and dKO-Hom mice. (**A**) MicroCT images of the proximal tibia (sagittal view) from the four groups of mice. (**B–F**) MicroCT quantification of BV/TV, density, Th.N, Tb.Th and Tb.Sp. dKO-Hom mice showed significantly lower BV/TV, Tb.N and Tb.Th, but higher Tb.Sp than WT, *mdx* and dKO-Het mice. Bone density was significantly lower in dKO-Hom than *mdx* and dKO-Het mice, and no significant differences were found when compared to WT mice. (**G**) Spine L6 trabecular bone (front view) from the four groups of mice. (**H–L**) MicroCT quantification showed significantly lower BV/TV, Tb.N and Tb.Th, but higher Tb.Sp, in dKO-Hom mice than in WT, *mdx* and dKO-Het mice. The BV density was significantly lower in dKO-Hom mice than in *mdx* and dKO-Het mice, but no significant difference was found when compared to the WT control group. (**M**) MicroCT 3D images of the femur midshaft. (**N**) Quantification of microCT of the femur midshaft indicated that the Ct.Th was significantly lower in dKO-Hom mice than in *mdx* and dKO-Het mice, but no significant differences were found between other groups. $^{*}P < 0.05$, $^{**}P < 0.01$, $^{***}P < 0.001$.

Osteopenia in dKO-Hom mice persists at 6 weeks of age

At 6 weeks of age, we examined muscle tissues from different parts of the body that surround bone tissues (skull, spine, femur and tibia muscle) in WT, *mdx*, dKO-Het and dKO-Hom mice, as performed with 4-week-old mice. Skeletal muscle necrosis, inflammation, heterotopic bone formation and fibrosis was also observed in *mdx*, dKO-Het and dKO-Hom mice (Fig. 6A). MicroCT results indicated that heterotopic bone formation was

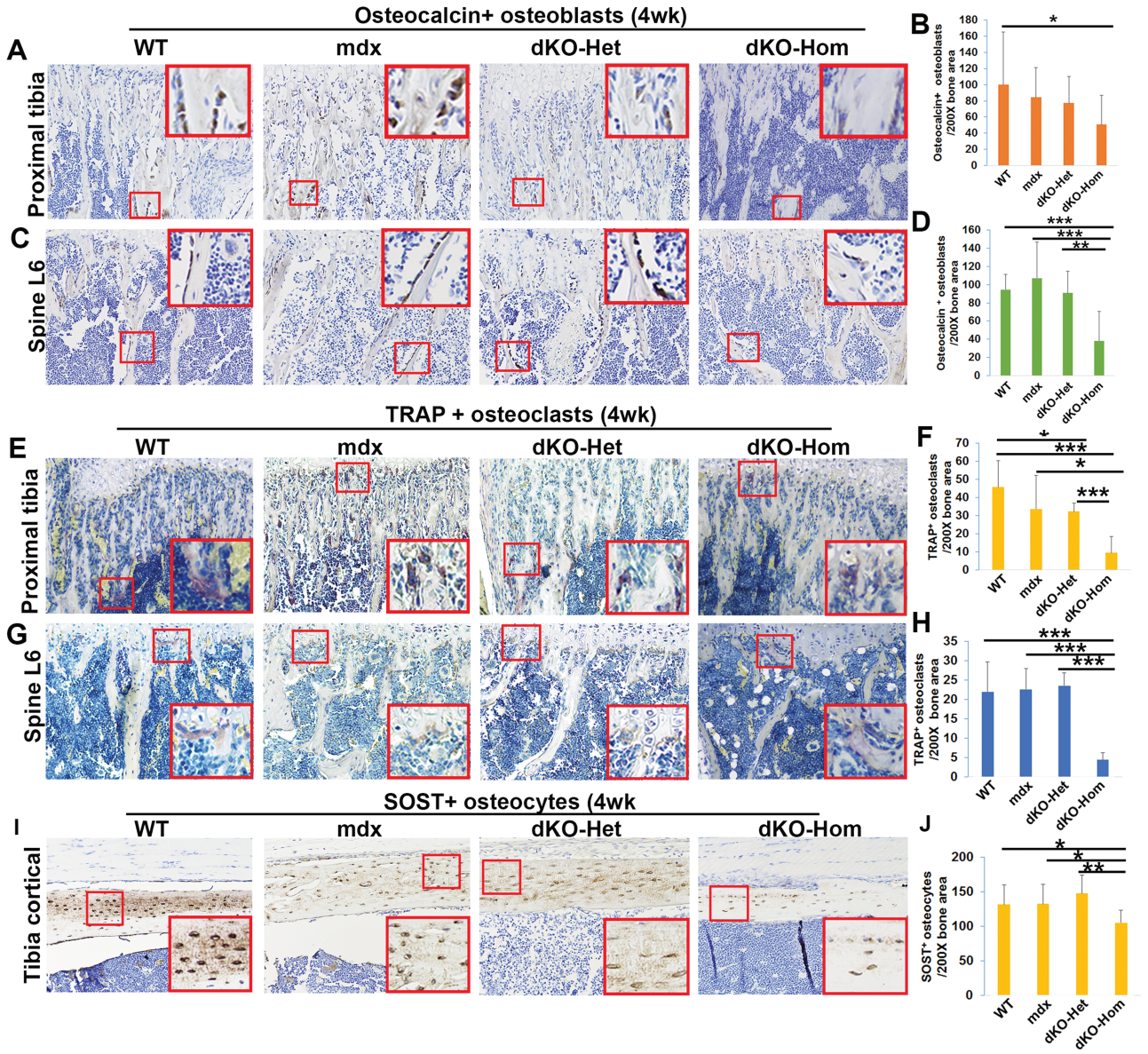

Figure 4. Immunohistochemical staining of osteoblasts, osteoclasts and osteocytes in bone tissue from 4-week-old WT, *mdx*, dKO-Het and dKO-Hom mice. (**A**) Representative images of osteocalcin staining of tissue from WT, mdx, dKO-Het and dKO-Hom mice show osteoblasts in the trabecular bone of the proximal tibia. (**B**) Quantification of osteocalcin staining indicated that the numbers of osteocalcin^{+} bone-lining osteoblasts were significantly lower in dKO-Hom mice than in WT control mice. (**C**) Representative images of osteocalcin staining of the spine L6. (**D**) Quantification of osteocalcin^{+} bone-lining osteoblasts in the spine L6 indicated that dKO-Hom mice had significantly fewer osteoblasts than WT, *mdx* and dKO-Het mice. (**E–F**) TRAP staining for osteoclasts and quantification in the proximal tibia. Osteoclast numbers were significantly decreased in the trabecular bone of the proximal tibia in dKO-Hom mice compared to those in WT, *mdx* and dKO-Het mice. Osteoclast numbers in trabecular bone of the proximal tibia in dKO-Het mice were also significantly lower than in WT control mice. (**G–H**) TRAP staining of osteoclasts in spine L6 and quantification. Osteoclast numbers were significantly lower in the trabecular bone of spine L6 of dKO-Hom mice than in WT, *mdx* and dKO-Het mice. (**I–J**) Quantification of osteocytes of tibia cortical bone. SOST^{+} osteocytes in the tibia cortical bone of dKO-Hom mice were significantly lower compared to those in WT, *mdx* and dKO-Het mice. Insets shown are the enlarged area of red boxes regions in each image which highlight positive cells. $^{*}P < 0.05$, $^{**}P < 0.01$, $^{***}P < 0.001$.

also present in the different skeletal muscle groups in the dKO-Hom, *mdx* and dKO-Het mice in contrast to WT skeletal muscle (Fig. 6B). MicroCT quantification of the proximal tibia indicated BV/TV was not significantly different in dKO-Hom mice compared to WT control mice, but was significantly lower in dKO-Hom mice than in *mdx* and dKO-Het mice (Fig. 7A–B). Bone density and Tb.N of the proximal tibia were significantly lower in dKO-Hom mice than in any of the other mouse groups (Fig. 7A, C–D), and no significant difference was found in Tb.Th among the four mouse groups tested (Fig. 7E). Although the Tb.Sp of trabecular bone of proximal tibia was significantly higher in dKO-Hom mice than in *mdx* and Het mice, no significant difference in Tb.Sp was found between dKO-Hom and WT mice (Fig. 7F). For the spine L6, the BV/TV and Tb.N were significantly lower in dKO-Hom mice than in any of the other groups, and Tb.Th was significantly lower in dKO-Hom relative to WT mice (Fig. 7G–H, J–K). The Tb.Sp was significantly higher in dKO-Hom mice than in any of the other mouse groups (Fig. 7L). The BV density of spine L6 in dKO-Hom mice was significantly lower than in *mdx* and dKO-Het mice, and no

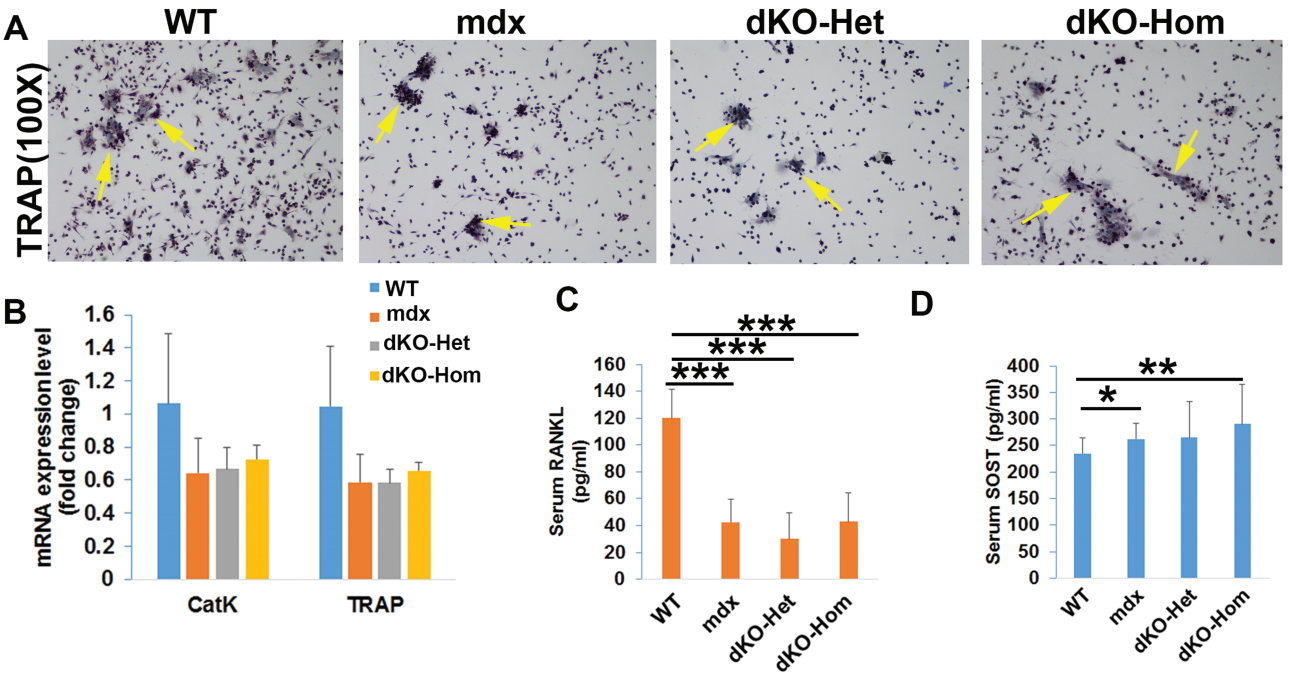

Figure 5. Mechanisms of impaired osteoclastogenesis in 4-week-old WT, *mdx*, dKO-Het and dKO-Hom mice. (**A**) TRAP staining of osteoclasts from 4-week-old mice after 7 days of culture. (**B**) Quantification of osteoclast gene expression at day 5 of osteoclastogenesis culture. *Mdx*, dKO-Het and dKO-Hom mice showed a trend toward decreased osteoclastogenesis compared to WT mice; however, these differences were not found to be statistically significant. (**C**) Serum RANKL was significantly decreased in *mdx*, dKO-Het and dKO-Hom mice compared to WT mice. (**D**) Serum SOST was significantly increased in dKO-Hom mice compared to WT control mice. *Mdx* mice also showed increased serum SOST levels relative to WT mice. $^{*}P < 0.05$, $^{**}P < 0.01$, $^{***}P < 0.001$.

significant difference was found between dKO-Hom and WT mice (Fig. 7I). Furthermore, we found that Ct.Th and density of the midshaft femur was significantly decreased in dKO-Hom mice relative to dKO-Het mice, but no differences were found when compared to WT and mdx mice (Fig. 7M–O). Histologically, H&E staining showed no significant differences between dKO-Hom and WT, *mdx* and dKO-Het mice in skull parietal bone (Supplementary Material, Fig. S10A). We found that the trabecular bone of dKO-Hom mice was sparse in spine L6 relative to WT, *mdx* and dKO-Het mice (Supplementary Material, Fig. S10B). We also found that the femur Ct.Th was thinner in dKO-Hom mice than in Het mice, and fewer trabeculae (Tb.N) were found in the proximal tibia of dKO-Hom mice than WT, *mdx* and dKO-Het mice (Supplementary Material, Fig. S10C–D). Herovici's staining indicated that there was no difference in collagen type I density in the skull trabecular bone among the four different mouse groups tested (Supplementary Material, Fig. S11A); however, collagen type I-positive trabeculae were more sparse in the spine L6 of dKO-Hom mice than WT, *mdx* and dKO-Het mice (Supplementary Material, Fig. S11B). Collagen type I-positive femur cortical bone was also thinner in dKO-Hom mice than dKO-Het mice (Supplementary Material, Fig. S11C). In addition, collagen type I-positive trabeculae in the proximal tibia were also fewer in dKO-Hom mice than in WT, *mdx* and dKO-Het mice (Supplementary Material, Fig. S11D).

Osteopenia in dKO-Hom mice at 6 weeks of age is associated with downregulation of osteoblastogenesis and upregulation of osteoclastogenesis

In order to investigate whether osteoblastogenesis and osteoclastogenesis is also affected at 6 weeks of age, we performed osteocalcin immunohistochemistry. We found that the osteocalcin-positive osteoblast number tended to be lower in the trabecular bone of the proximal tibia of dKO-Hom mice compared to WT mice ($P = 0.12$) (Fig. 8A–B). Strikingly, we found that osteoblast numbers in the trabecular bone of the spine L6 of dKO-Hom mice were significantly lower than WT, *mdx* and dKO-Het mice. The osteoblast number in trabecular bone of the spine L6 was also significantly lower in dKO-Het mice compared to WT mice (Fig. 8C–D). In contrast to our observations in 4-week-old mice, we found that the $TRAP^{+}$ osteoclast number in the proximal tibia was significantly increased in *mdx* and dKO-Het mice relative to WT mice. The number of osteoclasts in the proximal tibia of dKO-Hom mice also showed an increased trend (although not significant) relative to those in WT mice ($P = 0.075$, Wilcoxon rank sum test) (Fig. 8E–F). Furthermore, we found that the number of osteoclasts in the trabecular bone of spine L6 in dKO-Hom mice was significantly higher in dKO-Hom mice than in WT, *mdx* and dKO-Het mice (Fig. 8G–H). These results indicate that bone resorption was increased at this time point. However, the serum RANKL was significantly lower in *mdx*, dKO-Het and dKO-Hom mice than in WT mice. Furthermore, the serum level of SOST was significantly higher in *mdx*, dKO-Het and dKo-Hom mice, compared to WT mice.

Proteomic analysis of sera from normal and dKO-Hom mice

Based on proteomic analysis of sera from 4-week-old dKO-Hom and WT mice, we identified 124 proteins that were upregulated in dKO-Hom mice, with dKO-Hom to WT abundance score ratios >1.8. Our analysis indicates that 93 proteins were present only in the dKO-Hom mice. Thirty-one proteins had score ratios between 1.8 and 7.0 in dKO-Hom mice compared to control mice (Supplementary Material, Table S1). We further

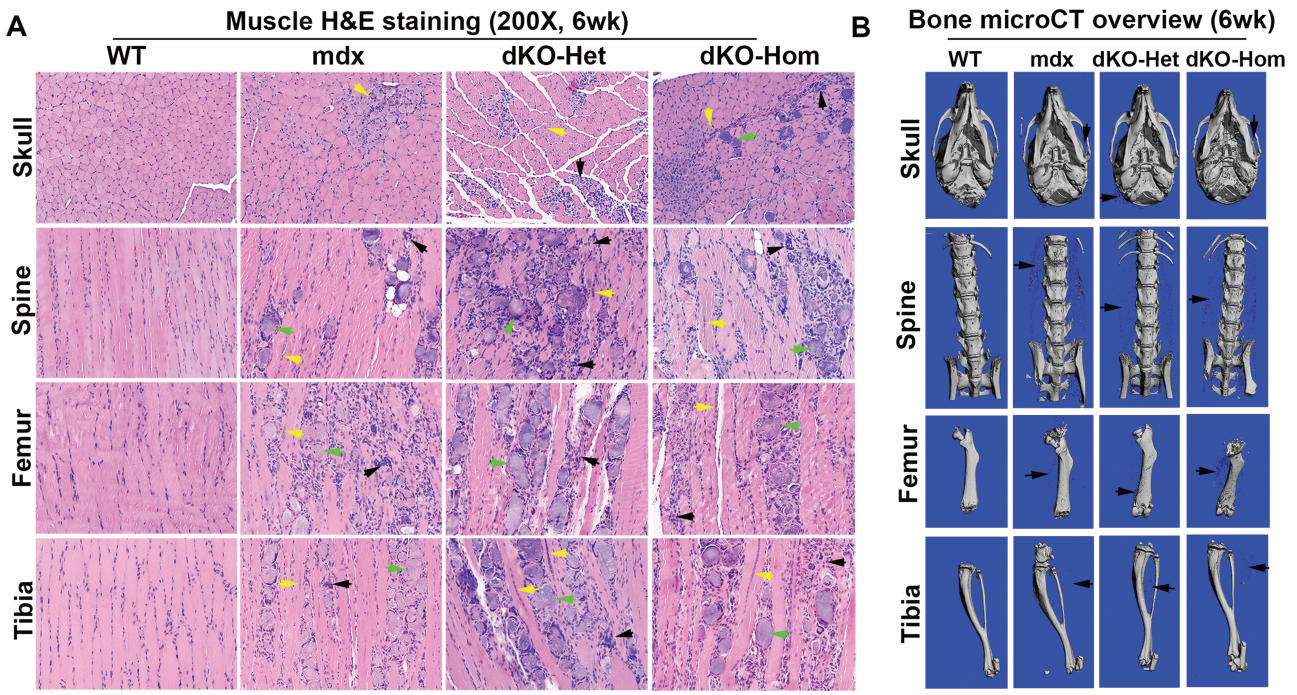

Figure 6. Characterization of muscle and bone of 6-week-old mice. (**A**) H&E staining (200×) of different skeletal muscle tissue from 6-week-old WT, mdx, dKO-Het and dKO-Hom mice. Severe muscle histopathology is evidenced by centrally nucleated myofibers and inflammation, and heterotopic bone formation is shown by the presence of bony structures. Yellow, green and black arrows point to the centrally nucleated myofiber, heterotopic bone structure and inflammation, respectively. (**B**) MicroCT 3D overview of bone tissue at 6 weeks of age. Bone structures of the skull, spine, femur and tibia of *mdx*, dKO-Het and dKO-Hom mice were similar to those of WT control mice; however, heterotopic bone formation in the soft tissue surrounding the bone tissue (black arrows) was obvious in the *mdx*, dKO-Het and dKO-Hom mice.

performed gene function annotation with the The Database for Annotation, Visualization and Integrated Discovery (DAVID) Annotation tool (20,21) (https://david.ncifcrf.gov/). We found that 35 of these proteins belong to glycoproteins. Furthermore, 178 proteins were downregulated in dKO-Hom mice compared to WT mice. Among these downregulated proteins, 23 had abundance score ratios of dKO-Hom to WT in the range of 0.174–0.6 (Supplementary Material, Table S2), and 155 proteins were found to be absent in WT mice. DAVID functional annotation results showed a group of 14 structural lens constituents and 9 visual perception-related genes were downregulated in dKO-Hom mice. Furthermore, three oxido-reductase activity proteins [NADH dehydrogenase (ubiquinone) Fe–S protein, cytochrome B5 reductase and superoxide dismutase 3] were downregulated in dKO-Hom mice. We also found four glycolysis-related proteins (enolase 2, gamma neuronal; enolase 3, beta muscle; glyceraldehyde-3-phosphatase dehydrogenase; and pyruvate kinase, muscle) downregulated in dKO-Hom mice compared to WT mice.

Discussion

In this study, we found that muscle histopathology in dKO-Hom mice occurred as early as 5 days of life, as demonstrated by centrally nucleated myofibers, muscle necrosis and inflammation in all muscle groups examined, relative to WT control mice. However, the onset of bone abnormalities in the dKO-Hom mice, as analyzed by microCT and histology, was not observed at 5 days of age, indicating that the onset of muscle pathology occurs earlier than that of bone pathology. Muscle histopathology persisted in the dKO-Hom mice at 2 weeks of age; however, bone microCT analysis showed only lower bone density in the proximal tibia of dKO-Hom mice at this age, compared to the other mouse groups. By 4 weeks of age, the muscle damage had become very severe, as demonstrated by severe muscle necrosis, inflammation, fibrosis and heterotopic bone formation. At this point, we found the bone quality of dKO-Hom mice to be significantly lower compared to WT, *mdx* and dKO-Het mice. Interestingly, *mdx* and dKO-Het mice did not show any bone abnormalities. Furthermore, we found that the numbers of osteoblasts and osteoclasts in the bone surface of the proximal tibia and spine were significantly lower in dKO-Hom mice than in WT, *mdx* and dKO-Het mice. No differences were found in osteoblast/osteoclast numbers in *mdx* and dKO-Het mice, compared to WT mice, at this time point. Osteocytes were also significantly lower in the tibia cortical bone of dKO-Hom mice relative to WT, mdx and dKO-Het mice. *In vitro* osteoclastogenesis showed a trend toward decreased levels of CatK and TRAP mRNA in dKO-hom, dKO-Het and *mdx* mice, compared to control. Correlated with this bone phenotype, we found that serum RANKL was lower in *mdx*, dKO-Het and dKO-Hom mice than in WT control mice. Serum SOST was higher in *mdx*, dKO-Het and dKO-Hom mice than in WT control mice. At 6 weeks of age, changes in muscle pathology persisted, similar to that seen at 4 weeks of age, and bone quality was also significantly lower in dKO-Hom mice than in WT, *mdx* and dKO-Het mice. At this time point, the osteoblast number was still lower in dKO-Hom mice than in WT, *mdx* and dKO-Het mice; however, the osteoclast number was increased in dKO-Hom, *mdx* and dKO-Het mice relative to WT control mice.

Reports from previous studies in humans have indicated that DMD patients always develop osteoporosis and have high risk of bone fracture due to decreased mobility and the corticosteroid intake that is often used to improve muscle function (22–24). The bone fracture risk in DMD patients is 20.9% in

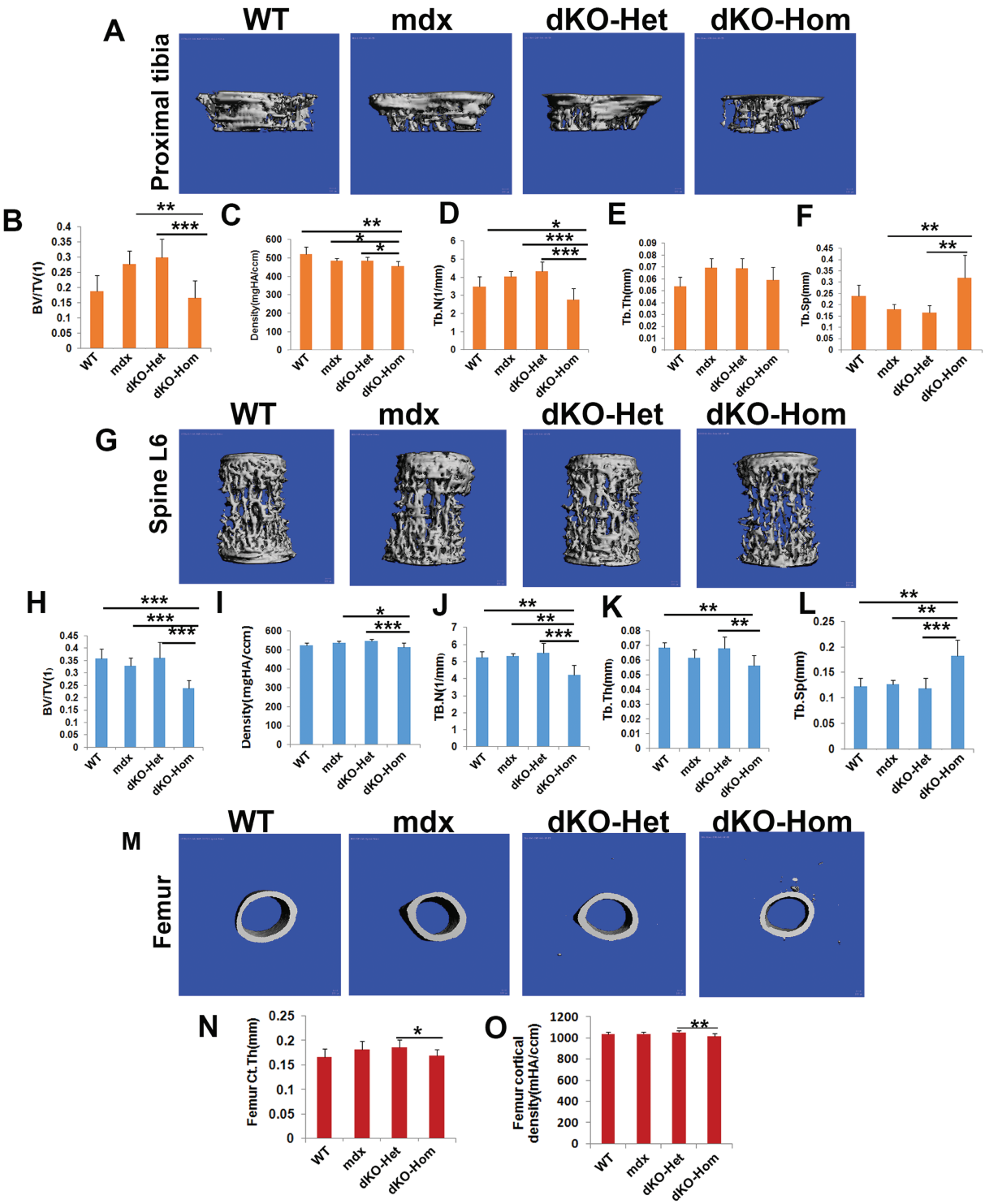

Figure 7. MicroCT analysis of bone tissue of 6-week-old WT, mdx, dKO-Het and dKO-Hom mice. (**A**). MicroCT 3D images of trabecular bone of the proximal tibia. (**B**) Quantification of BV/TV for the proximal tibia indicated there was significant reduction of BV/TV in dKO-Hom mice compared to *mdx* and dKO-Het mice, but no significant difference was found when compared to WT control mice. (**C**) Density of the proximal tibial trabecular bone was significantly lower in dKO-Hom mice compared to that of WT, *mdx* and dKO-Het mice. (**D**) Tb.N was significantly lower in the proximal tibia of dKO-Hom mice compared to WT, *mdx* and dKO-Het mice. (**E**) No significant differences in Tb.Th were found between dKO-Hom mice and the other groups. (**F**) The Tb.Sp was significantly higher in dKO-Hom mice than in *mdx* and dKO-Het mice. No significant difference between dKO-Hom and WT mice was found. (**G**) MicroCT 3D images of spine L6. (**H**) Quantification of microCT of spine L6 indicated that BV/TV was significantly lower in dKO-Hom mice than in WT, *mdx* and dKO-Het mice. (**I**) BV density of dKO-Hom mice was found to be significantly lower than that of *mdx* and dKO-Het mice, but not significantly different from that of WT mice. (**J**) The Tb.N of spine L6 was significantly lower in dKO-Hom mice than in WT, *mdx* and dKO-Het mice. (**K**) The Tb.Th of dKO-Hom mice was significantly lower than WT and DKO-Het mice. (**L**) The Tb.Sp of spine L6 was significantly higher in dKO-Hom mice than in WT, *mdx* and dKO-Het mice. (**M**) MicroCT 3D images of the midshaft femur cortical bone. (**N** and **O**). Quantification of microCT of the midshaft femur cortical bone indicated that thickness (Ct.Th) and bone density were significantly lower in dKO-Hom mice compared to dKO-Het mice, but no significant differences were found between dKO-Hom mice and WT or *mdx* mice. $^{*}P < 0.05$, $^{**}P < 0.01$, $^{***}P < 0.001$.

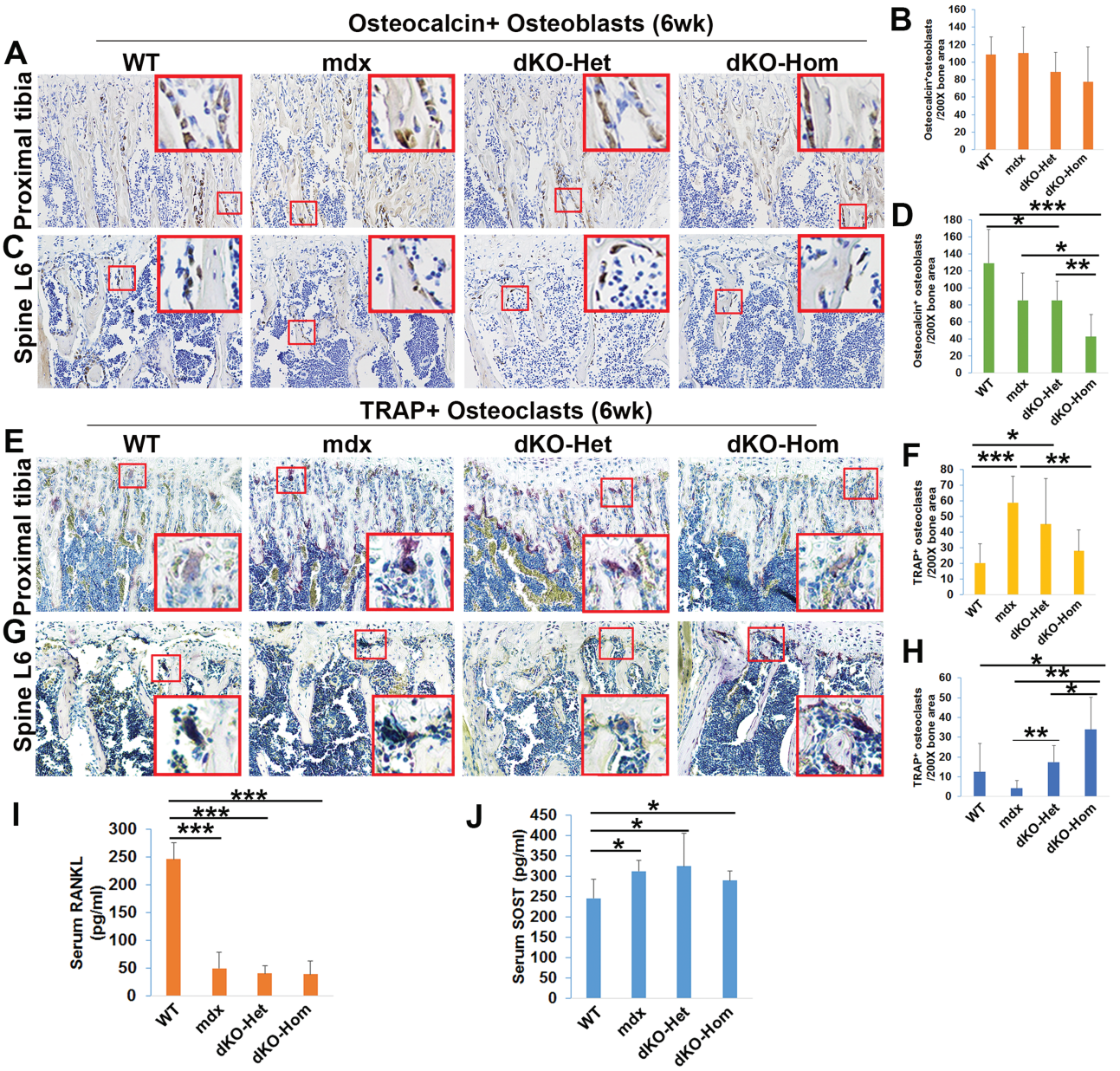

Figure 8. Immunohistochemistry staining of osteoblasts and osteoclasts in the proximal tibia and spine L6 of 6-week-old WT, *mdx*, dKO-Het and dKO-Hom mice. (**A**) Representative images of osteocalcin staining of trabecular bone of the proximal tibia in the four groups of mice to show osteoblasts. (**B**) Quantification indicated that the numbers of osteocalcin-positive osteoblasts appeared to be relatively lower in dKO-Hom mice than in WT mice, although the difference was not significant ($P = 0.12$). (**C**) Representative images of osteocalcin staining of the spine L6. (**D**) Quantification of osteocalcin-positive bone lining osteoblasts indicated there were significantly fewer osteocalcin-positive osteoblasts in dKO-Hom mice than in WT, *mdx* and dKO-Het mice. Furthermore, the number of osteocalcin-positive osteoblasts in dKO-Het mice was significantly lower than that in WT mice. (**E** and **F**) TRAP staining for osteoclasts and quantification of the proximal tibia. Osteoclast numbers were significantly increased in trabecular bone of the proximal tibia in *mdx* and dKO-Het mice compared to WT mice. The osteoclast number in the trabecular bone of the proximal tibia in dKO-Hom mice was significantly lower than in *mdx* mice. (**G** and **H**) TRAP staining for osteoclasts in spine L6 and quantification. Osteoclast number was significantly higher in the trabecular bone of spine L6 of dKO-Hom mice relative to those in WT, *mdx* and dKO-Het mice and significantly higher in DKO-Het relative to *mdx* mice. (**I**) Serum RANKL was significantly lower in *mdx*, dKO-Het and dKO-Hom mice compared to WT mice. $^{***}P < 0.001$. (**J**) Serum SOST level was significantly higher in *mdx*, dKO-Het and dKO-Hom mice compared to WT mice. $^{*}P < 0.05$.

ambulated patients and 29% of patients with bone fracture, using knee-ankle-foot orthoses, lost mobility permanently due to fracture (25). However, the low bone density that develops in DMD patients is often confounded by the use of corticosteroids, and the high risk of fractures poses a big health problem for DMD patients. In fact, following a bone fracture, DMD patients usually become wheelchair-bound; therefore, preserving bone homeostasis in DMD patients is very important to maintain the quality of life of those patients. Therefore, it is important to understand how the progression of the disease in DMD affects bone homeostasis.

The *mdx* mouse model is a murine model of human DMD. Its life span is relatively shorter than that of WT-C57BL10J mice (21–22 months versus 26–28 months) (26). However, the *mdx* mouse has a relatively mild phenotype of muscular dystrophy until late in life and does not mimic human DMD clinical manifestations.

The dKO-Hom mouse was first developed by J. R. Sanes' group. It has been shown to exhibit more severe cardiac and overall muscle dystrophy and is a more suitable model for investigating therapeutics for muscular dystrophy. The dKO-Hom mice are smaller at 4 weeks of age relative to WT mice, die at 4–14 weeks of age—50% of them die before 8 weeks of age—and they develop kyphosis and curved spine (12). It also has been shown that this model is more suitable for studies on gene therapy for DMD (13). Furthermore, our studies have shown that dKO-Hom mice demonstrate a more severe phenotype that includes muscle necrosis, stem cell depletion, fat infiltration, heterotopic bone formation and activation of Notch and RhoA/Rho-associated kinase (ROCK) signaling (14–16,18). Only a few studies of bone phenotype in muscular dystrophy mice have been reported. Nakagaki et *al*. (7) investigated the femur structure and biomechanical properties of 21-day-old *mdx* and control mice. They found that strength, stiffness and energy absorption were lower in *mdx* mice than in control mice, and femurs of *mdx* mice were shorter with smaller cortical area and thickness and a smaller area of epiphyseal trabecular bone (7). Another study showed that 6 month-old *mdx* mice demonstrated decreased bone mass, lower bone osteoblasts number and bone apposition rates and higher osteoclasts number and bone absorption markers when compared to WT mice. However, this study did not indicate the strain of control mice used for comparisons (8). In previous studies, we have also investigated the bone microarchitecture of the *mdx*, dKO-Het and dKO-Hom mice at 6–8 weeks of age. We have shown that dKO-Hom mice exhibited decreased bone density and Tb.Th relative to WT control mice, but no differences were found between *mdx*, dKO-Het and WT control mice (19).

In the current study, we further investigated timing of bone abnormalities during postnatal development and mechanisms of bone loss in dKO-Hom mice compared to that of *mdx*, dKO-Het and WT mice. We found that muscle histopathology occurred as early as 5 days after birth, while bone abnormalities were obvious by 4 weeks (and not at 5 days or 2 weeks) of age, as demonstrated by parallel comparison of muscle and bone histology as well as microCT. We found that, at 4 weeks of age, the dKO-Hom mice demonstrated significant decreases in trabecular BV/TV, Tb.N and Tb.Th compared to WT control, *mdx* and dKO-Het mice, for both the proximal tibia and spine, and no significant differences in these parameters were observed for *mdx* and dKO-Het mice compared to WT control mice. These results varied from the above-mentioned previous studies (7,8), which may be due to the fact that we used different ages of mice.

Furthermore, we found widespread heterotopic bone formation in all the dystrophic mouse skeletal muscle tissues examined (i.e. in *mdx*, dKO-Het and dKO-Hom mice). Interestingly, there is a paradox with respect to widespread heterotopic bone formation in skeletal muscles and osteopenia in the bones of dystrophic mice. Although it has been reported that heterotopic bone formation in *mdx* mice is caused by increased levels of serum inorganic phosphate (27), the mechanism behind heterotopic bone formation in the dystrophic musculature remains unclear.

Based on our finding that 4 weeks of age was a critical time by which bone abnormalities had developed in dystrophic mice, we further investigated the three critical types of cells involved in bone formation and absorption, at this time point. We found that the osteoblast number in trabecular bone surface of the proximal tibia and spine L6 was significantly lower, and osteoclast number was also significantly decreased, in dKO-Hom mice compared to WT control mice; on the other hand, *mdx* and dKO-Het mice did not exhibit statistically significant differences in these cell numbers compared to WT mice. These results indicate that dKO-Hom mice show bone growth retardation at 4 weeks of age compared to WT mice. In addition, we noticed that spine osteoblast and osteoclast changes were more profound than such changes observed in the proximal tibia. More importantly, we found that serum RANKL levels were significantly decreased in *mdx*, dKO-Het and dKO-Hom mice compared to WT control mice. These results are consistent with results found in DMD patients and in 6-month-old *mdx* mice, where RANKL levels in serum were also decreased (8). Lower serum RANKL levels may be associated with decreased osteoclasts in the trabecular bone of the proximal tibia and spine. Therefore, we performed osteoclastogenesis assays on bone marrow cells isolated from the femur and tibia of WT, *mdx*, dKO-Het and dKO-Hom mice. We found decreased osteoclastogenesis as demonstrated by TRAP staining at 7 days of culture and by quantitative polymerase chain reaction (Q-PCR) of CatK and TRAP expression at 5 days of differentiation in culture. The decrease in osteoblasts and osteoclasts may also represent an overall health span decline in dKO-Hom mice, due to severe muscle damage. However, it is not clear why bone quality was not decreased in the *mdx* and dKO-Het mice, even though these mice also demonstrated severe muscle damage at this time point. Previously, it has been reported that treatment for *mdx* mice at 5 and 6 weeks of age with pamidronate, an anti-absorptive bisphosphonate, increased cortical bone architecture and strength in femurs, resulting in increased resistance to bone fracture (28). However, this treatment did not improve overall bone growth in *mdx* mice and significantly inhibited bone remodeling in the metaphyseal trabecular bone, although muscle strength was improved (28). This suggests that increased bone absorption may not be the key mechanism for decreasing bone loss in dKO-Hom mice (28). RANKL, RANK and its decoy receptor Osteoprotegerin (OPG) have been used as targets for mitigating muscular dystrophy, and Osteoprotegerin/TNFRSF11B Full length chimera protein (OPG-FC) was found to be the most effective target for improving muscular dystrophy (29). This may support our finding that bone remodeling was actually decreased in dKO-Hom mice due to lower levels of serum RANKL.

We also found that serum SOST levels were increased in dKO-Hom mice compared to WT control mice. SOST is secreted by osteocytes and is an antagonist of Wnt signaling, playing a negative role in bone formation. SOST-specific antibody has been shown to be effective in improving bone mass in different patients in clinical trials (30), reversing ovariectomy-induced bone loss (31) and reducing bone loss of Wnt1 knockout mice (32). Therefore, the increase in serum SOST observed may also contribute to the osteopenia observed in dKO-Hom mice.

By 6 weeks of age, the muscle damage persisted, and bone microarchitecture parameters (such as BV/TV, density, Tb.N, Tb.Th, Tb.Sp) were also significantly lower for the proximal tibia, spine L6 and femur in dKO-Hom mice compared to WT mice. At this time point, we found that the osteoblast number in spine L6 was still significantly lower in dKO-Hom mice than in dKO-Het, *mdx* and WT control mice; however, the osteoclast number was significantly increased in the spine trabecular bone of dKO-Hom mice relative to dKO-Het, *mdx* and WT control mice. Furthermore, osteoclast numbers in the proximal tibia in *mdx* and dKO-Het mice were also significantly increased relative to WT mice; however, *mdx* and dKO-Het mouse bone parameters were not significantly changed compared to those of WT control mice. It appears that there is a dose-dependent change in osteoclast numbers in *mdx*, dKO-Het and dKO-Hom

mice. This is consistent with the results of a previous study of 6-month-old *mdx* mice (8).

Lastly, our proteomics data revealed differentially expressed proteins in dKO-Hom mice compared to WT mice. For example, we found fibulin-1 is increased in the serum of dKO-Hom mice compared to that of WT mice. It is an extra-cellular matrix that is important for bone formation and BMP2-induced osterix expression (33) and osteogenesis (34). Peroxiredoxin-2 negatively regulates osteoclast formation (35). The function of these genes in the development of the bone phenotype needs to be further investigated. Furthermore, we found that the serum structural constituent of lens and visual perception proteins are decreased in dKO-Hom mice compared to WT mice. These genes may be related to the eye symptoms seen in dKO-Hom mice. The decrease in oxidoreductase enzymes maybe related to impaired bone quality in dKO-Hom mice. However, the proteomics data did not reveal the change in RANKL and SOST levels observed using ELISA. This may be caused by a difference in sensitivity between proteomics and ELISA.

Conclusion

In summary, we found that dKO-Hom mice exhibit muscle damage as early as 5 days of life, while the bone abnormalities can be observed only at 4 weeks of age, when muscle damage, such as necrosis, heterotopic bone formation, inflammation and fibrosis are much more severe. Mechanistically, we found that the bone loss was due to decreased osteoblasts and osteoclasts and osteocytes number at 4 weeks of age in the dKO-Hom mouse model, which correlated with lower levels of RANKL and higher levels of SOST in serum. dKO-Hom mice recapitulate not only the muscle phenotype of human DMD, but also the bone phenotype of DMD. Whether muscle histopathologies cause osteopenia through myokines and osteokines profiles change in the muscle of dKO-Hom mice warrants further investigation.

Materials and Methods

Animal breeding

Dystrophin$^{-/-}$/utrophin$^{+/-}$ (dKO-Het) mice were obtained from Dr Bing Wang's laboratory at the University of Pittsburgh. The animals were housed and bred in the Association for Assessment and Accreditation of Laboratory Animal Care (AAALAC)-accredited UTHealth Center for Laboratory Animal Medicine and Care (CLAMC) animal facility to obtain the following three different genotypes of mice: (1) dystrophin$^{-/-}$/utrophin$^{+/+}$ (*mdx*), (2) dystrophin$^{-/-}$/utrophin$^{+/-}$ (dKO-Het) and (3) dystrophin$^{-/-}$/utrophin$^{-/-}$ (dKO-Hom) mice. Genotyping was performed using a Sigma RED PCR kit. C57BL10J WT mice were purchased from Jackson Laboratory for use as controls, and housed and bred in the UTHealth CLAMC animal facility in parallel with the dystrophic mice. To characterize bone microarchitecture, different groups of WT, *mdx*, dKO-Het and dKO-Hom mice were sacrificed at 5 days (N = 6–8), 2 weeks (N = 6–8), 4 weeks (N = 8–12) or 6 weeks of age (N = 6–8). Mice were anesthetized with 2% isoflurane, following a protocol approved by the UTHealth Animal Welfare Committee (AWC). Blood was collected from 4- and 6-week-old mice via the retro-orbital plexus just prior to sacrifice. Serum was isolated from whole blood using centrifugation methods and stored at −80°C until analysis. Immediately after sacrifice, skull, tibia, femur and spine tissues (bone and skeletal muscle) were dissected and then fixed with neutral buffered formalin for 48 h for subsequent analysis via microCT scanning and histology. All work with mice for this study was approved by the UTHealth AWC.

MicroCT scanning and analysis

After fixation of bone tissues, microCT scans were performed using a Viva CT 40 (Scanco Medical). The scanning resolution (15 μm) and protocol were kept consistent for all samples. MicroCT analysis was performed to reveal overview and for quantification of bone tissues. We analyzed the proximal tibia for trabecular bone and the spine trabecular bone of the entire lumbar 6 (spine L6). For the femur, we analyzed the cortical thickness. We chose the slices number of view of interest and threshold depending on animal age, because bone size and density are different during postnatal development. For the 5-day-old mouse proximal tibial trabecular bone analysis, we chose 30 of the 2D slices imaged right below the growth plate for quantification. We used Gauss = 0.8, Sigma = 1 and threshold = 120 for the trabecular bone of both proximal tibia and spine; we used 30 slices of midshaft of the femur and Gauss = 0.8, Sigma = 1 and threshold = 160 for femur cortical bone analysis. For 2-week-old mice, we chose 40 slices right below the growth plate for the proximal tibia analysis and Gauss = 0.8, Sigma = 1 and threshold = 140 parameters were used for proximal tibia and spine trabecular bone quantification. We analyzed 40 slices of femur cortical bone using Gauss = 0.8, Sigma = 1 and threshold = 180 for the midshaft of femur. For 4- and 6-week-old mice, we utilized 50 slices right beneath the growth plate and 50 slices for midshaft femur analysis. We used Gauss = 0.8, Sigma = 1 and threshold = 163 for trabecular bone of the proximal tibia and spine and Gauss = 0.8, Sigma = 1 and threshold = 200 for cortical bone analysis. Trabecular bone analysis was performed by carefully contouring the trabecular part of the proximal tibia and spine L6. All the bone parameters were generated by 3D evaluation software, and nomenclature followed the guidelines of the American Society of Bone and Mineral Research (36).

Histology

After microCT scanning, all samples were decalcified using 10% ethylenediaminetetraacidic acid (EDTA) disodium dehydrate and 1% sodium hydroxide (pH 7.0). H&E staining was performed on all samples. The muscle tissue that surrounded each part of the bone tissue was examined together with the bone tissues. TRAP staining was performed using a Sigma 387A kit following the manufacturer's protocol. Osteocalcin and SOST immunohistochemistry was also performed to identify osteoblasts and osteocytes, respectively. Herovici's staining was performed for all bone tissues, as previously described (37–39). Microscopic images were captured using a NIKON CI upright microscope. Quantification of TRAP-positive osteoclasts, osteocalcin-positive osteoblasts and SOST-positive osteocytes was performed using ImageJ software (NIH) and by measuring the bone area and normalizing to 200× field bone area for comparison between different groups.

Enzyme-linked immunosorbent assay

The serum concentrations of RANKL and SOST for 4- and 6-week-old mice in each of the four groups (WT, mdx, dKO-Het and dKO-Hom) were measured using a Mouse TRANCE/RANKL/TNFSF11 Quantikine ELISA Kit (MTR00) and Mouse/Rat SOST/Sclerostin Quantikine ELISA Kit (MSST00) (R&D systems), respectively, following the manufacturer's instructions.

In vitro osteoclastogenesis

Bone marrow cells were flushed out from the tibial and femoral bone marrow of mice from each of the four groups using Phosphate buffered saline (PBS) supplemented with 2% fetal bovine serum, and cells were titrated to single cells, filtered through a 70 µm cell strainer and seeded into T25 flasks. After 24 h of culture, non-adhering cells were transferred to another T25 flask and stimulated with 100 ng/ml of monocyte (macrophage)-colony stimulating factor (M-CSF) to promote monocyte–macrophage proliferation. After 3 days of culture, macrophages were trypsinized with 0.25% trypsin-EDTA for 40 min and cells were resuspended in osteoclast differentiation medium containing RANKL (50 ng/ml) and M-CSF (100 ng/ml) for osteoclastogenesis and then seeded in 12-well plates with cover glass for TRAP staining, or without cover glass for reverse transcriptase quantitative PCR (RT-qPCR), as described previously (40,41). Osteoclast differentiation was detected using TRAP staining (7 days of culture) and RT-qPCR for TRAP and CatK (5 days of culture). The following primers were designed using Primer3 software (42,43) and used for PCR; TRAP forward primer: 5′-CAGCAGCCAAGGAGGACTAC-3′, TRAP reverse primer: 5′-ACATAGCCCACACCGTTCTC-3′, CatK forward primer: 5′-CCAGTGGGAGCTATGGAAGA-3′, CatK reverse primer, 5′-TGGTTCATGGCCAGTTCATA-3′.

Proteomics

Liquid chromatography–mass spectrometry (LC-MS) analysis of sera from 4-week-old dKO-Hom and WT mice was used to identify differentially expressed proteins. LC-MS was carried out by the Proteomics Core facility at the Institute of Molecular Medicine, McGovern Medical School at UTHealth. The abundance score was compared between dKO-Hom and WT mice. The ratios of abundance scores for dKO-Hom mice to control mice that were >1.8 or <0.6 were considered upregulated and downregulated proteins, respectively.

Statistical analysis

Power analyses were performed to determine the number of animals required for each experiment, based on the proposed parameters and using software available online (https://www.stat.ubc.ca/~rollin/stats/ssize/n2.html).

The alpha value was set at 0.05 and the beta value was set at 0.80. For experimental results, two-sided tests were used. Analysis of variance or the Student's *t*-test was used to compare multiple groups or two groups, respectively. $P < 0.05$ was considered statistically significant. The Wilcoxon rank sum test was used for data that exhibited high variability.

Supplementary Material

Supplementary Material is available at HMG online.

Acknowledgements

We thank Dr Mary A. Hall and Dr Lavanya Rajagopalan for scientific and English editing of the manuscript.

Conflict of Interest statement. None declared.

Funding

National Institute of Health of USA (NIH) [1R01AR065445 to J.H.] and start-up funds at UTHealth and Steadman Philippon Research Institute.

Authors' roles

Study design: J.H., X.G. Study conduct: X.G., Y.T., S.A., X.S., H.C., B.W. Data collection: X.G. Data analysis: X.G. Data interpretation: X.G., J.H. Drafting manuscript: X.G. Revising manuscript content: J.H. Approving final version of manuscript: J.H., X.G., B.W., Y.T., S.A., X.S., H.C. J.H. takes responsibility for the integrity of the data analysis.

References

1. Koenig, M., Hoffman, E.P., Bertelson, C.J., Monaco, A.P., Feener, C. and Kunkel, L.M. (1987) Complete cloning of the Duchenne muscular dystrophy (DMD) cDNA and preliminary genomic organization of the DMD gene in normal and affected individuals. *Cell*, **50**, 509–517.
2. Hoffman, E.P., Monaco, A.P., Feener, C.C. and Kunkel, L.M. (1987) Conservation of the Duchenne muscular dystrophy gene in mice and humans. *Science*, **238**, 347–350.
3. Hoffman, E.P., Brown, R.H. Jr. and Kunkel, L.M. (1987) Dystrophin: the protein product of the Duchenne muscular dystrophy locus. *Cell*, **51**, 919–928.
4. Hoffman, E.P., Fischbeck, K.H., Brown, R.H., Johnson, M., Medori, R., Loike, J.D., Harris, J.B., Waterston, R., Brooke, M., Specht, L. *et al*. (1988) Characterization of dystrophin in muscle-biopsy specimens from patients with Duchenne's or Becker's muscular dystrophy. *N. Engl. J. Med*., **318**, 1363–1368.
5. Darras, B.T., Harper, J.F. and Francke, U. (1987) Prenatal diagnosis and detection of carriers with DNA probes in Duchenne's muscular dystrophy. *N. Engl. J. Med*., **316**, 985–992.
6. Sicinski, P., Geng, Y., Ryder-Cook, A.S., Barnard, E.A., Darlison, M.G. and Barnard, P.J. (1989) The molecular basis of muscular dystrophy in the mdx mouse: a point mutation. *Science*, **244**, 1578–1580.
7. Nakagaki, W.R., Bertran, C.A., Matsumura, C.Y., Santo-Neto, H. and Camilli, J.A. (2011) Mechanical, biochemical and morphometric alterations in the femur of mdx mice. *Bone*, **48**, 372–379.
8. Rufo, A., Del Fattore, A., Capulli, M., Carvello, F., De Pasquale, L., Ferrari, S., Pierroz, D., Morandi, L., De Simone, M., Rucci, N. *et al*. (2011) Mechanisms inducing low bone density in Duchenne muscular dystrophy in mice and humans. *J. Bone Miner. Res*., **26**, 1891–1903.
9. Abou-Khalil, R., Yang, F., Mortreux, M., Lieu, S., Yu, Y.Y., Wurmser, M., Pereira, C., Relaix, F., Miclau, T., Marcucio, R.S. *et al*. (2014) Delayed bone regeneration is linked to chronic inflammation in murine muscular dystrophy. *J. Bone Miner. Res*., **29**, 304–315.
10. Nakagaki, W.R. and Camilli, J.A. (2012) Spontaneous healing capacity of calvarial bone defects in mdx mice. *Anat. Rec. (Hoboken)*, **295**, 590–596.
11. Novotny, S.A., Warren, G.L., Lin, A.S., Guldberg, R.E., Baltgalvis, K.A. and Lowe, D.A. (2012) Prednisolone treatment and restricted physical activity further compromise bone of mdx mice. *J. Musculoskelet. Neuronal Interact*., **12**, 16–23.
12. Grady, R.M., Teng, H., Nichol, M.C., Cunningham, J.C., Wilkinson, R.S. and Sanes, J.R. (1997) Skeletal and cardiac myopathies in mice lacking utrophin and dystrophin: a model for Duchenne muscular dystrophy. *Cell*, **90**, 729–738.
13. Wang, B., Li, J., Fu, F.H. and Xiao, X. (2009) Systemic human minidystrophin gene transfer improves functions and life span of dystrophin and dystrophin/utrophin-deficient mice. *J. Orthop. Res*., **27**, 421–426.
14. Mu, X., Usas, A., Tang, Y., Lu, A., Wang, B., Weiss, K. and Huard, J. (2013) RhoA mediates defective stem cell function

and heterotopic ossification in dystrophic muscle of mice. *FASEB J.*, **27**, 3619–3631.
15. Lu, A., Poddar, M., Tang, Y., Proto, J.D., Sohn, J., Mu, X., Oyster, N., Wang, B. and Huard, J. (2014) Rapid depletion of muscle progenitor cells in dystrophic mdx/utrophin−/− mice. *Hum. Mol. Genet.*, **23**, 4786–4800.
16. Mu, X., Tang, Y., Lu, A., Takayama, K., Usas, A., Wang, B., Weiss, K. and Huard, J. (2015) The role of Notch signaling in muscle progenitor cell depletion and the rapid onset of histopathology in muscular dystrophy. *Hum. Mol. Genet.*, **24**, 2923–2937.
17. Sohn, J., Lu, A., Tang, Y., Wang, B. and Huard, J. (2015) Activation of non-myogenic mesenchymal stem cells during the disease progression in dystrophic dystrophin/utrophin knockout mice. *Hum. Mol. Genet.*, **24**, 3814–3829.
18. Mu, X., Tang, Y., Takayama, K., Chen, W., Lu, A., Wang, B., Weiss, K. and Huard, J. (2017) RhoA/ROCK inhibition improves the beneficial effects of glucocorticoid treatment in dystrophic muscle: implications for stem cell depletion. *Hum. Mol. Genet.*, **26**, 2813–2824.
19. Isaac, C., Wright, A., Usas, A., Li, H., Tang, Y., Mu, X., Greco, N., Dong, Q., Vo, N., Kang, J. *et al.* (2013) Dystrophin and utrophin 'double knockout' dystrophic mice exhibit a spectrum of degenerative musculoskeletal abnormalities. *J. Orthop. Res.*, **31**, 343–349.
20. Huang da, W., Sherman, B.T. and Lempicki, R.A. (2009) Systematic and integrative analysis of large gene lists using DAVID bioinformatics resources. *Nat. Protoc.*, **4**, 44–57.
21. Huang da, W., Sherman, B.T. and Lempicki, R.A. (2009) Bioinformatics enrichment tools: paths toward the comprehensive functional analysis of large gene lists. *Nucleic Acids Res.*, **37**, 1–13.
22. Ma, J., McMillan, H.J., Karaguzel, G., Goodin, C., Wasson, J., Matzinger, M.A., DesClouds, P., Cram, D., Page, M., Konji, V.N. *et al.* (2017) The time to and determinants of first fractures in boys with Duchenne muscular dystrophy. *Osteoporos. Int.*, **28**, 597–608.
23. Barzegar, M., Niknam, E., Habibi, P., Shiva, S. and Tahmasebi, S. (2018) Bone mineral density and bone metabolism in patients with Duchenne muscular dystrophy. *Iran J. Child Neurol.*, **12**, 77–83.
24. Singh, A., Schaeffer, E.K. and Reilly, C.W. (2018) Vertebral fractures in Duchenne muscular dystrophy patients managed with deflazacort. *J. Pediatr. Orthop.*, **38**, 320–324.
25. McDonald, D.G., Kinali, M., Gallagher, A.C., Mercuri, E., Muntoni, F., Roper, H., Jardine, P., Jones, D.H. and Pike, M.G. (2002) Fracture prevalence in Duchenne muscular dystrophy. *Dev. Med. Child Neurol.*, **44**, 695–698.
26. Chamberlain, J.S., Metzger, J., Reyes, M., Townsend, D. and Faulkner, J.A. (2007) Dystrophin-deficient mdx mice display a reduced life span and are susceptible to spontaneous rhabdomyosarcoma. *FASEB J.*, **21**, 2195–2204.
27. Kikkawa, N., Ohno, T., Nagata, Y., Shiozuka, M., Kogure, T. and Matsuda, R. (2009) Ectopic calcification is caused by elevated levels of serum inorganic phosphate in mdx mice. *Cell Struct. Funct.*, **34**, 77–88.
28. Yoon, S.H., Sugamori, K.S., Grynpas, M.D. and Mitchell, J. (2016) Positive effects of bisphosphonates on bone and muscle in a mouse model of Duchenne muscular dystrophy. *Neuromuscul. Disord.*, **26**, 73–84.
29. Dufresne, S.S., Boulanger-Piette, A., Bosse, S., Argaw, A., Hamoudi, D., Marcadet, L., Gamu, D., Fajardo, V.A., Yagita, H., Penninger, J.M. *et al.* (2018) Genetic deletion of muscle RANK or selective inhibition of RANKL is not as effective as full-length OPG-fc in mitigating muscular dystrophy. *Acta Neuropathol. Commun.*, **6**, 31.
30. Appelman-Dijkstra, N.M. and Papapoulos, S.E. (2016) Sclerostin inhibition in the management of osteoporosis. *Calcif. Tissue Int.*, **98**, 370–380.
31. Li, X., Ominsky, M.S., Villasenor, K.S., Niu, Q.T., Asuncion, F.J., Xia, X., Grisanti, M., Wronski, T.J., Simonet, W.S. and Ke, H.Z. (2018) Sclerostin antibody reverses bone loss by increasing bone formation and decreasing bone resorption in a rat model of male osteoporosis. *Endocrinology*, **159**, 260–271.
32. Joeng, K.S., Lee, Y.C., Lim, J., Chen, Y., Jiang, M.M., Munivez, E., Ambrose, C. and Lee, B.H. (2017) Osteocyte-specific WNT1 regulates osteoblast function during bone homeostasis. *J. Clin. Invest.*, **127**, 2678–2688.
33. Cooley, M.A., Harikrishnan, K., Oppel, J.A., Miler, S.F., Barth, J.L., Haycraft, C.J., Reddy, S.V. and Scott Argraves, W. (2014) Fibulin-1 is required for bone formation and Bmp-2-mediated induction of osterix. *Bone*, **69**, 30–38.
34. Hang Pham, L.B., Yoo, Y.R., Park, S.H., Back, S.A., Kim, S.W., Bjorge, I., Mano, J. and Jang, J.H. (2017) Investigating the effect of fibulin-1 on the differentiation of human nasal inferior turbinate-derived mesenchymal stem cells into osteoblasts. *J. Biomed. Mater. Res. A*, **105**, 2291–2298.
35. Park, H., Noh, A.L., Kang, J.H., Sim, J.S., Lee, D.S. and Yim, M. (2015) Peroxiredoxin II negatively regulates lipopolysaccharide-induced osteoclast formation and bone loss via JNK and STAT3. *Antioxid. Redox Signal.*, **22**, 63–77.
36. Bouxsein, M.L., Boyd, S.K., Christiansen, B.A., Guldberg, R.E., Jepsen, K.J. and Muller, R. (2010) Guidelines for assessment of bone microstructure in rodents using micro-computed tomography. *J. Bone Miner. Res.*, **25**, 1468–1486.
37. Turner, N.J., Pezzone, M.A., Brown, B.N. and Badylak, S.F. (2013) Quantitative multispectral imaging of Herovici's polychrome for the assessment of collagen content and tissue remodelling. *J. Tissue Eng. Regen. Med.*, **7**, 139–148.
38. Gao, X., Usas, A., Lu, A., Kozemchak, A., Tang, Y., Poddar, M., Sun, X., Cummins, J.H. and Huard, J. (2016) Cyclooxygenase-2 deficiency impairs muscle-derived stem cell-mediated bone regeneration via cellular autonomous and non-autonomous mechanisms. *Hum. Mol. Genet.*, **25**, 3216–3231.
39. Gao, X., Usas, A., Proto, J.D., Lu, A., Cummins, J.H., Proctor, A., Chen, C.W. and Huard, J. (2014) Role of donor and host cells in muscle-derived stem cell-mediated bone repair: differentiation vs. paracrine effects. *FASEB J.*, **28**, 3792–3809.
40. Cui, S., Xiong, F., Hong, Y., Jung, J.U., Li, X.S., Liu, J.Z., Yan, R., Mei, L., Feng, X. and Xiong, W.C. (2011) APPswe/Abeta regulation of osteoclast activation and RAGE expression in an age-dependent manner. *J. Bone Miner. Res.*, **26**, 1084–1098.
41. Lee, Y., Kim, H.J., Park, C.K., Kim, Y.G., Lee, H.J., Kim, J.Y. and Kim, H.H. (2013) MicroRNA-124 regulates osteoclast differentiation. *Bone*, **56**, 383–389.
42. Untergasser, A., Cutcutache, I., Koressaar, T., Ye, J., Faircloth, B.C., Remm, M. and Rozen, S.G. (2012) Primer3—new capabilities and interfaces. *Nucleic Acids Res.*, **40**, e115.
43. Koressaar, T. and Remm, M. (2007) Enhancements and modifications of primer design program Primer3. *Bioinformatics*, **23**, 1289–1291.